SSRG International Journal of Geo-informatics and Geological Science
ISSN: 2393–9206 / https://doi.org/10.14445/23939206/IJGGS-V12I2P101

Volume 12 Issue 2, 1-8, May-Aug 2025
© 2025 Seventh Sense Research Group®

*Research Article*

# Land Surface Temperature Estimation from Satellite Imagery in Imphal-Iril River Catchment, Manipur, India

Ngangom Robertson[1], Oinam Bakimchandra[2]

[1,2]*Department of Civil Engineering, NIT Manipur, Imphal, India.*

[1]*Corresponding Author : robertson.nitm@gmail.com*

Received: 01 May 2025 Revised: 02 June 2025 Accepted: 18 June 2025 Published: 03 July 2025

***Abstract*** *- One of the most essential parameters for any climate model is land surface temperature, which is also regarded as an important indicator for the assessment of global energy balance and hydrologic modeling. The Imphal-Iril River catchment is the present study area where agricultural land (16.5%) and forest (73%) are the most prevalent Land Use Land Cover (LULC) classifications. The main objective of this research is to assess the spatial variation of land surface temperature (LST) across various land use types within the catchment by using satellite-based normalized difference vegetation index (NDVI) and land surface emissivity (LSE). LST was derived using ArcGIS 10.3 from the thermal infrared sensor (TIRS) Band 10 of Landsat 8 imagery for three different periods, namely 22 November 2018, 8 December 2018, and 9 January 2019. The present study used 45 in situ observations for various land uses and the MODIS LST product to validate the computed LST. The results reveal that LST estimated from Landsat 8 has an excellent correlation with in situ LST observation data. The study also observed that a negative relationship exists between NDVI and LST for all periods. The spatial patterns of LST were assessed across three time periods to gain insight into surface temperature fluctuations in the area.*

***Keywords*** *- Geographic information system, Land surface emissivity, Land surface temperature, NDVI, MODIS.*

## 1. Introduction

The temperature of the Earth's surface, which may be measured when it comes into direct contact with a measurement device, is known as land surface temperature (LST). LST, often referred to as the "skin temperature" of the Earth's surface, plays a vital role in urban climate research [1]. It significantly influences the Earth's physical, chemical, and biological systems, making it an essential parameter in environmental studies [2]. LST is widely used in a number of scientific research activities and is a crucial variable for detecting surface temperature, particularly in urban areas, calculating energy consumption in buildings, and assessing heat-related problems [3]. LST is connected to surface energy and water balance and has primary importance in a wide range of applications such as urban climate, climate change, vegetation monitoring, and hydrological cycles. Air temperature and LST are important indicators in the study of climate change, hydrology, energy balance, and biodiversity. Several variables influence LST, including vegetation, soil moisture, elevation, terrain, topography, and so on [4]. LST is sensitive to a wide range of land surface attributes and may be utilized for collecting information and data on various LULC classes [5]. It may also be used for monitoring agricultural drought by giving surface temperature data for the region [6]. With the growing realization of the significance of LST, many methods for estimating it have been developed. Radiometric temperature is derived from the surface-emitted radiance and calculated using the radiative emission equation. It is identical to the thermodynamic temperature for isothermal surfaces. Because satellite remote sensing provides a repeating synoptic picture of the Earth's surface in short intervals, it is an important tool for monitoring the LST of a region [7]. Urbanization has been highlighted as one of the major contributors to climate change, causing a serious environmental concern [8, 9]. Agricultural areas, water bodies, and barren land have all been drastically reduced owing to significant population growth [10]. Landsat 8 carries two onboard sensors: the Operational Land Imager (OLI) and the Thermal Infrared Sensor (TIRS). While ground-based surveys can yield highly precise information, they are often labour-intensive, expensive, and challenging to conduct, making remote sensing a more practical and widely favored alternative [11, 12]. In regional-scale research, remote sensing techniques are presently capable of offering extensive spatial and temporal coverage [13]. Utilizing remote sensing techniques alongside geographic information systems (GIS) has become a key method for detecting and analyzing environmental changes over time [14]. Researchers worldwide frequently rely on remote sensing data to assess land surface temperature and surface emissivity with accuracy and efficiency. A variation in

LST is observed when vegetation region is converted into non-vegetative usage, and it has contributed a direct impact on global warming [15, 16]. With extensive spatial coverage and frequent revisit capabilities, satellite observations provide the ability to measure LST globally at a pixel-based average scale [17]. An increase in LST significantly impacts the climatic patterns of monsoon-dominated countries, often resulting in unpredictable rainfall. This disruption in precipitation patterns can adversely affect vegetation growth and distribution across the Earth's surface [18].

Earlier, LST was estimated using a few ground-based sample points, with values interpolated into isotherms to represent an area. With the advancement of remote sensing, thermal satellite data now allows for more accurate, efficient, and large-scale LST estimation. LST is extensively utilized across multiple disciplines. It plays a crucial role in estimating evapotranspiration, examining climate variability, understanding hydrological processes, evaluating vegetation conditions, investigating urban thermal environments, and supporting environmental studies. [19]. Thermal remote sensing technology has increasingly become a valuable tool in precision agriculture, aiding in the detection of crop water stress, identification of plant diseases, and efficient management of irrigation practices [20, 21].

Despite significant advancements in remote sensing techniques, accurate estimation of LST remains a challenge due to limitations such as atmospheric interference, surface emissivity variability, urban heterogeneity, and coarse spatial resolution of satellite data. Moreover, existing models often lack reliability across diverse land cover types and climatic conditions. This study aims to overcome these challenges by developing enhanced techniques for precise and high-resolution LST estimation through the integration of remote sensing and GIS approaches. This study focuses on the integration of multi-temporal satellite imagery with high-resolution GIS-based analysis to estimate land surface temperature in a complex terrain. The main objective of this study is to estimate Land Surface Temperature (LST) using the thermal band of Landsat 8 satellite imagery. The computed LST is verified through comparison with ground measurements and the MODIS daily LST dataset. Additionally, the relationship between LST and the Normalized Difference Vegetation Index (NDVI) within the study area is analyzed.

## 2. Study Area

Manipur lies in the northeastern part of India and is recognized for its diverse landscape and ecological significance. The state is geographically situated between latitudes 23.83°N and 25.68°N and longitudes 93.03°E and 94.78°E. It focuses on the Imphal–Iril river catchment, which covers nearly 1,830 square kilometres and experiences an average yearly rainfall of approximately 1,467 mm. As shown in Figure 1, the region includes a range of elevations from 732 m to 2,676 m and is traversed by two significant rivers, namely the Imphal and Iril rivers that flow through the basin. The hilly regions are predominantly covered with medium to dense tropical deciduous forests. The catchment area comprises various land cover types, such as croplands, forested areas, human settlements, exposed soil, and surface water bodies. The livelihood and economic stability of many residents in Manipur are closely tied to agricultural activities, with more than 75% of the population employed in agriculture and its related sectors, and the state experiences a humid climate, although it is marked by seasonal water scarcity [22].

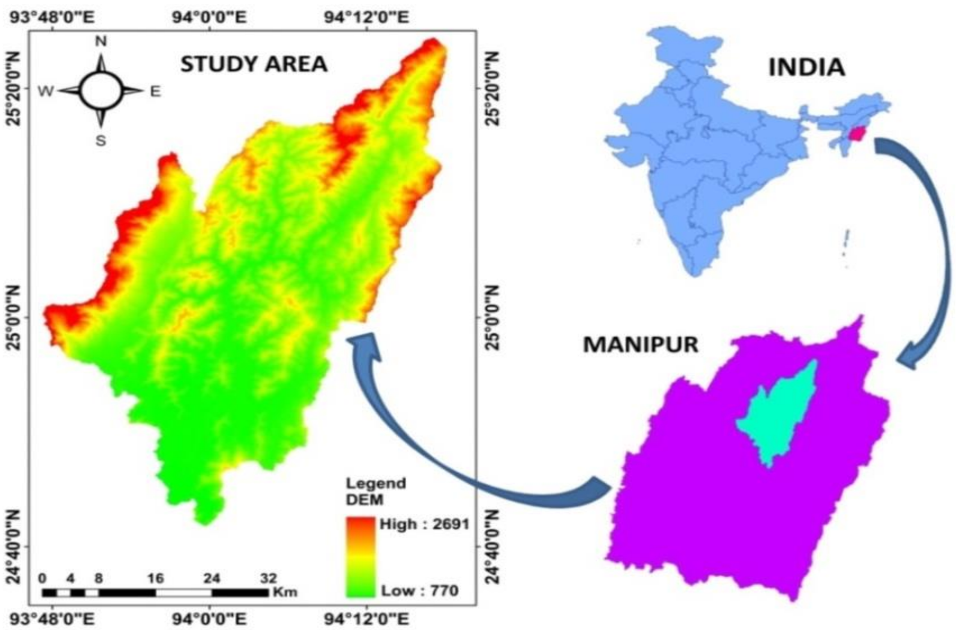


**Fig. 1 Geospatial context of the study site**

**Table 1. Description of Landsat-8**

| Band No. | Designation | Wavelength | Spatial Resolution |
|---|---|---|---|
| 2 | Blue | 0.45 – 0.51 µm | 30 m |
| 3 | Green | 0.53 – 0.59 µm | 30 m |
| 4 | Red | 0.64 – 0.67 µm | 30 m |
| 5 | Infrared | 0.85 – 0.88 µm | 30 m |
| 10 | Thermal Infrared | 10.6 – 11.19 µm | 30 m |

*Source: USGS*

## 3. Data Used

### *3.1. Multispectral Data*

The multispectral remote sensing images of Landsat 8(OLI+TIRS) of the study area were collected from the USGS Earth Explorer site. Landsat-8 satellite imagery provides spatial data with a revisit cycle of every 16 days, offering consistent temporal resolution for monitoring changes over time. This study utilized satellite imagery from three separate dates: 22 November 2018, 8 December 2018, and 9 January 2019 (daytime, Level-1G product, path/row 135/42 and 135/43). The LST was derived using the Thermal Infrared Sensor (TIRS) Band 10 of Landsat 8 through ArcGIS tools. The NDVI was calculated from Landsat 8 OLI data using Band 5 (Near Infrared) and Band 4 (Red). All datasets were reprojected to the Universal Transverse Mercator (UTM) coordinate system, specifically WGS-84, having zone 46N.

### *3.2. In-situ Data*

A Spectrum soil thermometer was employed to record in situ LST across various land use categories. For each observation period, forty-five ground sampling points were selected using a random sampling approach, ensuring representation of all land cover types. These on-site soil temperature readings were utilized to validate satellite-derived LST and to create a continuous LST surface for the study region. The portable soil thermometer facilitated real-time surface temperature measurements at a soil depth ranging from 0 to 5 cm. Prior to data collection, the device was calibrated, offering a measurement accuracy of plus or minus 1.8 °C.

### *3.3. MODIS LST Data*

The MODIS MOD11A1 data product was additionally utilized to verify the estimated LST. These datasets can be freely accessed through the USGS archive at https://lpdaac.usgs.gov/. While the nominal spatial resolution of this product is 1 km, the actual resolution applied in this study corresponded to a grid size of approximately 1,200 km. The data is then resampled to 30 m resolution to achieve homogeneity with Landsat 8 imaging data. MODIS LST daily data from three different periods were used: 22 November 2018, 8 December 2018, and 9 January 2019.

## 4. Methodology

Figure 2 presents the flowchart outlining the procedure for estimating LST. This methodology is implemented using Landsat 8 satellite data with the support of ArcGIS tools and analytical techniques. The brightness temperature is derived from Band 10 of the TIRS, while the Normalized NDVI is computed using Bands 4 and 5 from the Operational Land Imager (OLI). A detailed explanation of each step involved in generating the LST is provided in the following section.

### *4.1. Conversion into Radiance*

The data from Landsat 8 TIRS Band 10 (thermal band) was transformed into spectral radiance using the radiance rescaling coefficients provided in the accompanying metadata file. This spectral radiance was then used to calculate the brightness temperature [23, 24].

$$\text{Spectral radiance, } L\lambda = ML * Qcal + AL \qquad (1)$$

Where $Q_{\mathrm{cal}}$ is the Pixel value (DN), $M_{\mathrm{L}}$and $A_{\mathrm{L}}$ are rescaling coefficient values.

### *4.2. Brightness Temperature*

With the conversion of DN values to sensor spectral radiance, the TIRS band 10 data is then converted to brightness temperature (BT) using the thermal constants provided in the metadata file, as shown in Equation (2) [24, 25].

$$\mathrm{BT} = \frac{\mathrm{K2}}{\ln[(\mathrm{k1}/\mathrm{L}\lambda)+1] - 273.15} \qquad (2)$$

The thermal constants K1 and K2, associated with Landsat 8 TIRS Band 10, are available in the metadata file accompanying the satellite imagery. To convert the calculated brightness temperature from Kelvin to Celsius, absolute zero (approximately - 273.15°C) must be subtracted from the temperature values.

### *4.3. NDVI Calculation*

The NDVI is calculated using Landsat imagery by applying a formula that divides the difference between the near-infrared (NIR) and red (RED) bands by their combined total, as represented in Equation (3) [26].

$$\mathrm{NDVI} = \frac{\mathrm{NIR-RED}}{\mathrm{NIR+RED}} \qquad (3)$$

NDVI is one of the most widely adopted vegetation indices derived from satellite imagery for assessing vegetation cover across a region [27]. The values range from -1 to +1 and are computed by taking the normalized ratio of the difference between the Near-Infrared (NIR) and Red bands for each pixel. An NDVI value of zero typically corresponds to water bodies. Values below 0.2 generally indicate areas with little to no vegetation, such as bare soil. Surfaces with NDVI values below 0.5 are considered to have full vegetation coverage. When NDVI values fall between 0.1 and 0.5, the land surface is interpreted as being a mixture of vegetation and bare soil [28].

### *4.4. Proportion of Vegetation*

The next step is to compute proportional vegetation (Pv) using the information obtained from NDVI values. This proportional vegetation provides an estimate of the area covered by each land cover class.

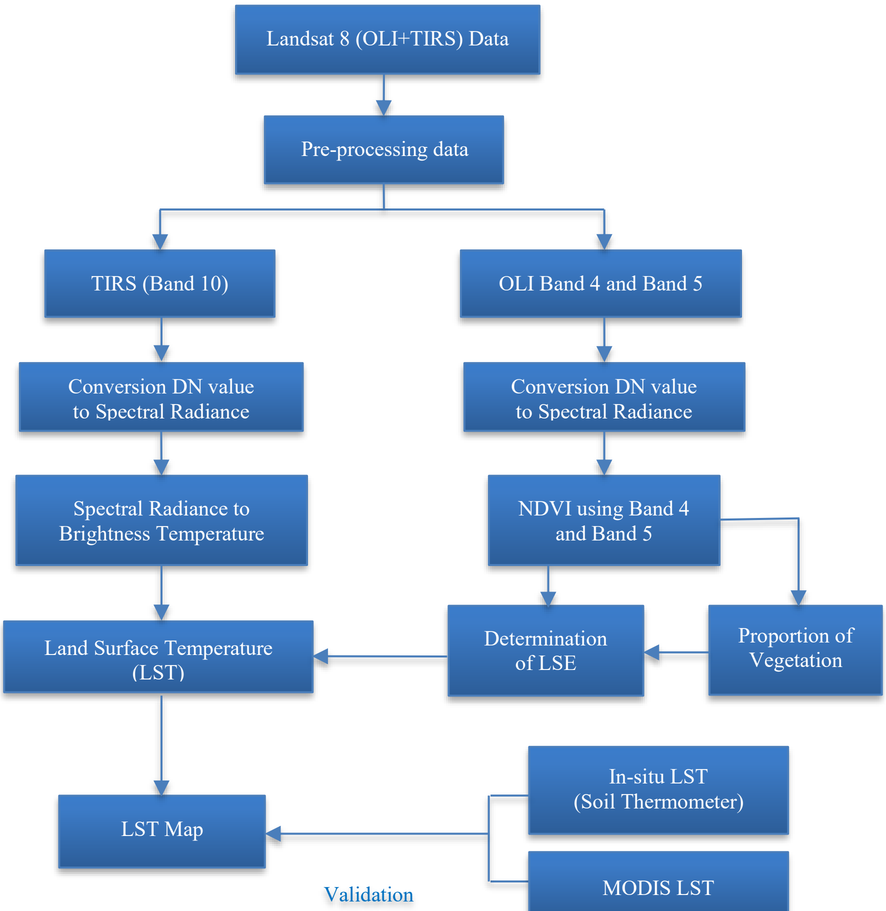


**Fig. 2 Data processing flow chart for LST**

The fraction of vegetation and bare soil cover is estimated using NDVI values from reference (or pure) pixels. For global-scale analyses, standard NDVI values are typically set at NDVIv = 0.5 for fully vegetated surfaces and NDVIs =0.2 for bare soil. However, in high-resolution agricultural imagery, the NDVI value for dense vegetation (NDVIv) can be significantly higher, often reaching 0.8 or even 0.9. The proportion of vegetation cover (Pv) is then determined using the formula presented in Equation (4). [29].

$$Pv = [\frac{(NDVI-NDVIs)}{(NDVIv-NDVIs)}]^2 \quad (4)$$

### *4.5. Computation of Land Surface Emissivity (LSE)*

LSE plays a key role in detecting emitted radiation and transferring thermal energy to the atmosphere [30]. Natural surfaces typically exhibit variability in LSE due to their heterogeneous characteristics, which are mainly influenced by surface texture and the type of vegetation present. The emissivity of vegetated areas is significantly affected by factors such as plant species, growth stage, and vegetation density [31]. In comparison to terrestrial surfaces, the emissivity of water surfaces is nearly constant. In this study, the NDVI threshold method was applied to calculate the emissivity of various land uses in the 10-12 µm range using Equation (5) [32].

$$\begin{array}{ll} \lambda_{\varepsilon\lambda} = \varepsilon_{s\lambda} & NDVI < NDVI_s \\ \varepsilon_{v\lambda}P_v + \varepsilon_{s\lambda}(1 - P_v) + C_\lambda, & NDVI_s \leq NDVI \geq NDVI_v \\ \varepsilon_{s\lambda} + C_\lambda, & NDVI > NDVI_v \end{array} \quad (5)$$

Where εv and εs denote the emissivity values of vegetation and soil, respectively, while C represents surface roughness, assigned a constant value of 0.005. When the NDVI is less than 0, the surface is classified as a water body and is given an emissivity of 0.991.

For NDVI values ranging from 0 to 0.2, the land is categorized as bare soil with an emissivity of 0.966. NDVI values between 0.2 and 0.5 indicate a mix of vegetation and soil cover. Surfaces with NDVI greater than 0.5 are considered fully vegetated and are attributed an emissivity value of 0.973.

***4.6 Derivation of LST***

LST is estimated using the brightness temperature derived from Band 10 of the thermal infrared sensor and computed LSE, which is also derived from Pv and NDVI [33, 34]. As a result, LST can be calculated using Equation (6).

$$\mathrm{LST} = \frac{\mathrm{TB}}{1+(\lambda * \mathrm{BT}/\rho)\mathrm{In}(\varepsilon)} \quad (6)$$

Where, TB represents the brightness temperature in degrees Celsius, $\boldsymbol{\lambda}$ denotes the wavelength corresponding to Band 10, ε stands for land surface emissivity, and ρ is a constant with a value of 1.438 × 10² mK.

## 5. Results and Discussion

***5.1. Analysis of computed LST and observed LST***

LST for the three selected dates was derived from Landsat 8 satellite imagery and is illustrated in Figure 3. On 22 November 2018, areas classified as settlements exhibited noticeably higher LST values compared to regions under agriculture, vegetation, and forest cover. The cooler surface temperatures recorded in agricultural zones during this time are attributed to higher soil moisture content. On 8 December 2018 and 9 January 2019, both settlement and agricultural regions demonstrated elevated LST, whereas forested and vegetated zones maintained lower temperatures. The rise in LST across agricultural lands is likely due to reduced moisture levels and the absence of farming activity, leaving the soil bare and fully exposed to solar radiation.

To assess the accuracy of the estimated LST, a total of 45 ground-truth data points were collected across the three dates and compared with the satellite-derived temperatures, as depicted in Figure 4. The results revealed a strong positive correlation between the field observations and the estimated LST, with coefficient of determination ($R^2$) values of 0.65, 0.69, and 0.78 for 22 November 2018, 8 December 2018, and 9 January 2019, respectively, and showing a possible difference of plus or minus 2°C.

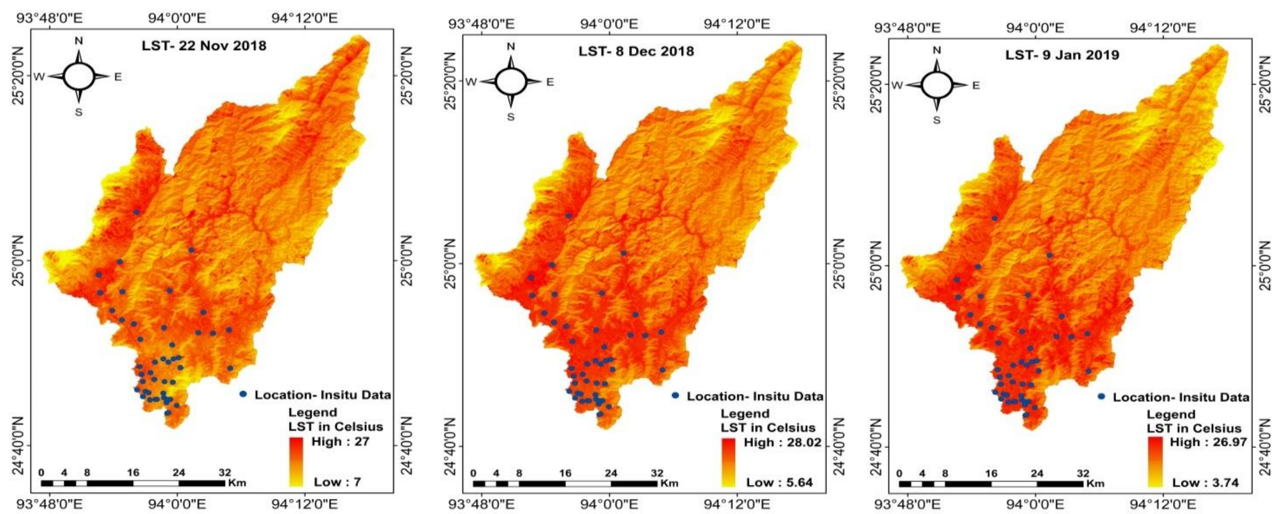


**Fig. 3 LST map for 3 different periods**

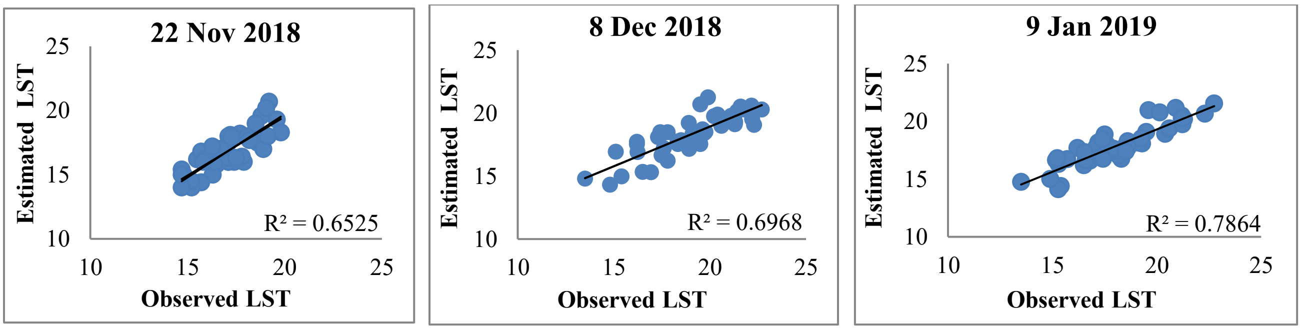


**Fig. 4 Scatter plot of observed and estimated LST**

***5.2. Comparison of Derived LST with MODIS-LST***

The computed LST from the thermal band of Landsat 8 was compared with the daily Global 1 km Terra MODIS LST data product. MODIS (MOD11A1) LST layers for three different periods were extracted. The estimated LST is plotted against each other using 45 relevant sites, which are shown in Figure 5. The plotted graph revealed a low value of $R^2$ for all three time periods since the spatial resolution of MODIS LST data is quite coarse (1 km), and LST layers estimated from Landsat 8 thermal band seemed to have a resolution of 30 m. From the regression model, $R^2$ values for 22 November 2018, 8 December 2018, and 9 January 2019 are 0.42, 0.51 and 0.49, respectively. Every pixel in the MODIS LST image represents an area of 1 km x 1 km, but each image in the Landsat 8 image covers only an area of 30 m x 30 m and causes scaling effects. As a result, the estimated LST from Landsat 8 and the MODIS LST product cannot be completely matched to the corresponding pixel value. Thus, less correlation between the computed LST and the MODIS LST data product is observed in all periods.

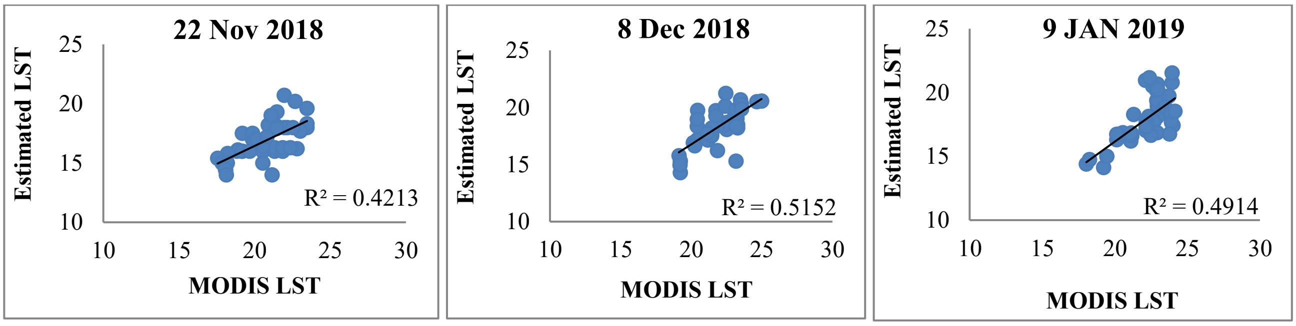


**Fig. 5 Plots the graph of MODIS LST vs Estimated LST**

### *5.3. Correlation between LST and NDVI*

To analyze the strength of the relationship between NDVI and LST, forty-five NDVI values representing various land use types were plotted against the corresponding computed LST values. As illustrated in Figure 6, the results indicate a notable inverse correlation between NDVI and LST, with $R^2$ values recorded as 0.30, 0.49, and 0.36 for 22 November 2018, 8 December 2018, and 9 January 2019, respectively. This suggests that as NDVI increases, indicating denser vegetation, the associated LST tends to decrease. Conversely, lower NDVI values correspond to higher surface temperatures.

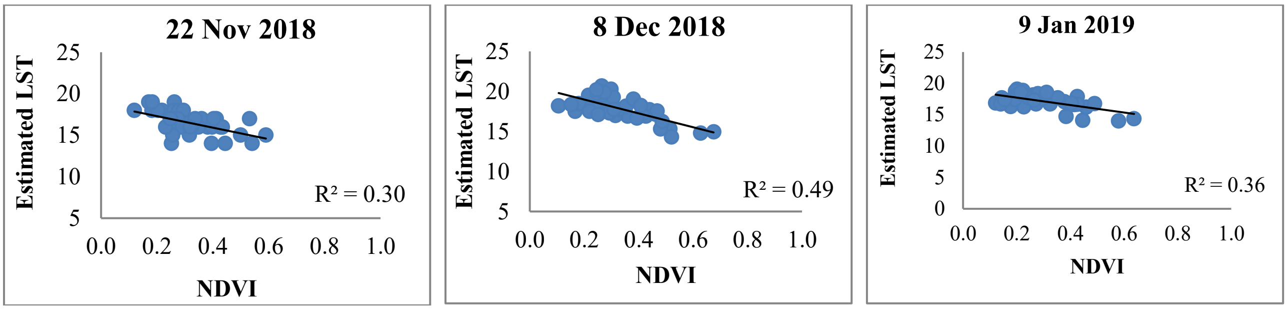


**Fig. 6 Graph of NDVI - LST for 22 November 2018, 8 December 2018 and 9 January 2019**

## 6. Conclusion

In this study, LST distribution maps were generated using Landsat 8 TIRS satellite imagery with the aid of ArcGIS 10.3. The methodology involved calculating brightness temperature from Band 10 of the TIRS sensor and estimating surface emissivity based on land cover types, utilizing both visible and infrared bands from Landsat 8 data. The derived LST values were validated against ground-based measurements obtained with a Spectrum portable soil thermometer and the MODIS daily LST product. The validation results demonstrated a strong correlation between the estimated and observed LST values, indicating the reliability of this approach for regional or large-scale LST mapping. Additionally, the analysis showed a meaningful inverse relationship between LST and NDVI, confirming that vegetation cover influences surface temperature. Future research can apply similar methods across different seasons to better understand temporal variations in LST. Furthermore, this framework could be adapted for modeling continuous soil moisture levels within the study area using the integrated LST–NDVI approach. This sort of research is critical for understanding the evolution of urban heat, which has a significant influence on the environment. LST also serves as a key parameter in observing and supporting the development of sustainable agricultural practices within the region.

## Acknowledgements

The authors acknowledge the United States Geological Survey (USGS) for providing access to essential datasets used in this study and extend heartfelt thanks to the National Institute of Technology Manipur for its continuous support and motivation throughout the research process.

## References

[1] Janak P. Joshi, and Bindu Bhatt, "Estimating Temporal Land Surface Temperature Using Remote Sensing: A Study of Vadodara Urban Area, Gujarat," *International Journal of Geology, Earth & Environmental Sciences*, vol. 2, no.1, pp. 123-130, 2012. [Google Scholar] [Publisher Link]

[2] Ruiliang Pu et al., "Assessment of Multi-Resolution and Multi-Sensor Data for Urban Surface Temperature Retrieval," *Remote Sensing of Environment*, vol. 104, no. 2, pp. 211-225, 2006. [CrossRef] [Google Scholar] [Publisher Link]
[3] Aneesh Mathew et al., "Prediction of Surface Temperatures for the Assessment of Urban Heat Island Effect Over Ahmedabad City Using Linear Time Series Model," *Energy and Buildings*, vol. 128, pp. 605-616, 2016. [CrossRef] [Google Scholar] [Publisher Link]
[4] Yen-Jen Lai et al., "Comparison of MODIS Land Surface Temperature and Ground – Based Observed Air Temperature in Complex Topography," *International Journal of Remote Sensing*, vol. 33, no. 24, pp. 7685-7702, 2012. [CrossRef] [Google Scholar] [Publisher Link]
[5] Suman Sinha, Laxmi Kant Sharma, and Mahendra Singh Nathawat, "Improved Land-Use/Land-Cover Classification of Semi-Arid Deciduous Forest Landscape Using Thermal Remote Sensing," *Egyptian Journal of Remote Sensing and Space Sciences*, vol. 18, pp. 217-233, 2015. [CrossRef] [Google Scholar] [Publisher Link]
[6] Amal Yahya Alshaikh, "Space Applications for Drought Assessment in Wada-Dama (West Tabouk), KSA," *Egyptian Journal Remote Sensing and Space Science*, vol. 18, no. 1, pp. 543-553, 2015. [CrossRef] [Google Scholar] [Publisher Link]
[7] Offer Rozenstein et al., "Derivation of Land Surface for Landsat-8 TIRS Using a split Window Algorithm," *Sensors*, vol. 14, no. 4, pp. 5768-5780, 2014. [CrossRef] [Google Scholar] [Publisher Link]
[8] Mark P. McCarthy, Martin J. Best, and Richard A. Betts, "Climate Change in Cities Due to Global Warming and Urban Effects," *Geophysical Research Letters*, vol. 37, no. 9, pp. 1-5, 2010. [CrossRef] [Google Scholar] [Publisher Link]
[9] Xiao-Ling Chen et al., "Remote Sensing Image-Based Analysis of the Relationship between Urban Heat Island and Land Use/Cover Changes," *Remote Sensing of Environment*, vol. 104, no. 2, pp. 133-146, 2006. [CrossRef] [Google Scholar] [Publisher Link]
[10] Hassan Mohammadian Mosammam et al., "Monitoring Land Use Change and Measuring Urban Sprawl Based on Its Spatial Forms: The Case of Qom City," *Egyptian Journal of Remote Sensing and Space Sciences*, vol. 20, no. 1, pp. 103-116, 2017. [CrossRef] [Google Scholar] [Publisher Link]
[11] Juan C. Jiménez-Muñoz et al., "Land Surface Temperature Retrieval Methods from Landsat-8 Thermal Infrared Sensor Data," *IEEE Geoscience Remote Sensing Letters*, vol. 11, no. 10, pp. 1840-1843, 2014. [CrossRef] [Google Scholar] [Publisher Link]
[12] Charlie J. Tomlinson et al., "Remote Sensing Land Surface Temperature for Meteorology and Climatology: A Review," *Meteorological Applications*, vol. 18, no. 3, pp. 296-306, 2011. [CrossRef] [Google Scholar] [Publisher Link]
[13] Chen Shulin, Liu Yuanbo, and Wen Zuomin, "Satellite Retrieval of Soil Moisture: An Overview," *Advances in Earth Science*, vol. 27, no. 11, pp. 1192-1203, 2012. [CrossRef] [Google Scholar] [Publisher Link]
[14] Cheolmin Kim, "Land Use Classification and Land Use Change Analysis Using Satellite Images in Lombok Island, Indonesia," *Journal of Science and Technology*, vol. 12, no. 4, pp. 183-191, 2016. [CrossRef] [Google Scholar] [Publisher Link]
[15] Patricia Wanjiku Mwangi, Faith Njoki Karanja, and Peter Kariuki Kamau, "Analysis of the relationship between land surface temperature and vegetation and built-up indices in upper-hill, Nairobi," *Journal of Geoscience and Environment Protection*, vol. 6, no. 1, pp. 1-16, 2018. [CrossRef] [Google Scholar] [Publisher Link]
[16] S. Anbazhagan, and C.R. Paramasivam, "Statistical Correlation Between Land Surface Temperature (LST) and Vegetation Index (NDVI) Using Multi-Temporal Landsat TM Data," *International Journal of Advance Earth Science and Engineering*, vol. 5, no. 1, pp. 333-346, 2016. [Google Scholar] [Publisher Link]
[17] Wei Zhao, and Zhao-Liang Li, "Sensitivity Study of Soil Moisture on the Temporal Evolution of Surface Temperature Over Bare Surfaces," *International Journal of Remote Sensing*, vol. 34, no. 9-10, pp. 3314-3331, 2013. [CrossRef] [Google Scholar] [Publisher Link]
[18] A. Rajeshwari, and N.D. Mani, "Estimation of Land Surface Temperature of Dindigul District Using Landsat 8 Data," *International Journal of Research in Engineering and Technology*, vol. 3, no. 5, pp. 122-126, 2014. [CrossRef] [Google Scholar] [Publisher Link]
[19] Vijay Solanky, Sangeeta Singh, and S. K. Katiyar, "Land Surface Temperature Estimation Using Remote Sensing Data," *Hydrologic Modeling*, vol. 81, pp. 343-351, 2018. [CrossRef] [Google Scholar] [Publisher Link]
[20] Sami Khanal, John Fulton, and Scott Shearer, "An Overview of Current and Potential Applications of Thermal Remote Sensing in Precision Agriculture," *Computers and Electronics in Agriculture*, vol. 139, pp. 22-32, 2017. [CrossRef] [Google Scholar] [Publisher Link]
[21] Grazia Tucci et al., "Multi-Sensor UAV Application for Thermal Analysis on a Dry-Stone Terraced Vineyard in Rural Tuscany Landscape," *ISPRS International Journal of Geo-Information*, vol. 8, no. 2, pp. 1-21s, 2019. [CrossRef] [Google Scholar] [Publisher Link]
[22] T.K. Sen et al., Soil Erosion of Manipur, NBSS Publication, 2006. [Google Scholar]
[23] Raghad Nasier Hussain, and Rana Mozahim, "Assessment of Land-sat Satellite Images used to calculate Land Surface Temperature (LST): A case study in Adhamiya Baghdad," *IOP Conference Series, Earth and Environmental Science*, vol. 1300, pp. 1-20, 2024. [CrossRef] [Google Scholar] [Publisher Link]
[24] Landsat Missions, United States Geological Survey, Landsat 8 (L8) Data Users Handbook, Version 2 Department of the Interior, U.S. Geological Survey, 2016. [Online]. Available: https://www.usgs.gov/landsat-missions/landsat-8-data-users-handbook

[25] D. Jeevalakshmi, S. Narayana Reddy, and B. Manikiam, “Land Surface Temperature Retrieval From LANDSAT Data Using Emissivity Estimation,” *International Journal of Applied Engineering Research*, vol. 12, pp. 9679-9687, 2017. [Google Scholar] [Publisher Link]

[26] Hao Zhang et al., “NDVI-Net: A Fusion Network for Generating High-Resolution Normalized Difference Vegetation Index in Remote Sensing,” *ISPRS Journal of Photogrammetry and Remote Sensing*, vol. 168, pp. 182-196, 2020. [CrossRef] [Google Scholar] [Publisher Link]

[27] Fei Yuan, and Marvin E. Bauer, “Comparison of Impervious Surface Area and Normalized Difference Vegetation Index as Indicators of Surface Urban Heat Island Effects in Landsat Imagery,” *Remote Sensing of Environment*, vol. 106, no. 3, pp. 375-386, 2007. [CrossRef] [Google Scholar] [Publisher Link]

[28] Wenxia Qiu, Huixi Xu, and Zhengwei He, “Study on the Difference of Urban Heat Island Defined by Brightness Temperature and Land Surface Temperature Retrieved by RS Technology,” *Journal Computer Modeling and New Technologies*, vol. 18, no. 4, pp. 222-225, 2014. [Google Scholar] [Publisher Link]

[29] Fei Wang et al., “An Improved Mono-Window Algorithm for Land Surface Temperature Retrieval from Landsat 8 Thermal Infrared Sensor Data,” *Remote Sensing*, vol. 7, no. 4, pp. 4268-4289, 2015. [CrossRef] [Google Scholar] [Publisher Link]

[30] Ugur Avdan, and Gordana Jovanovska, “Algorithm for Automated Mapping of Land Surface Temperature Using Landsat 8 Satellite Data,” *Journal of Sensors*, vol. 2016, no. 1, pp. 1- 8, 2016. [CrossRef] [Google Scholar] [Publisher Link]

[31] Yong-Gang Qian, Zhao-Liang Li, and Françoise Nerry, “Evaluation of Land Surface Temperature and Emissivities Retrieved from MSG/SEVIRI Data with MODIS Land Surface Temperature and Emissivity Products,” *International Journal of Remote Sensing*, vol. 34, pp. 3140-3152, 2013. [CrossRef] [Google Scholar] [Publisher Link]

[32] Jose A. Sobrino et al., “Land Surface Emissivity Retrieval from Different VNIR and TIR Sensors,” *IEEE Transactions on Geoscience and Remote Sensing*, vol. 46, no. 2, pp. 316-327, 2008. [CrossRef] [Google Scholar] [Publisher Link]

[33] Marina Stathopoulou, and Constantinos Cartalis, “Daytime urban heat islands from Landsat ETM+ and Corine land cover data: An application to major cities in Greece,” *Solar Energy*, vol. 81, no. 3, pp. 358-368, 2007. [CrossRef] [Google Scholar] [Publisher Link]

[34] United States Geological Survey, Landsat 8 (L8) Data Users Handbook, LSDS-1574, Version 1.0, 2015. [Google Scholar]